Inclusive Production of the ω and η Mesons in Z Decays, and the Muonic Branching Ratio of the ω

The ALEPH Collaboration[*)]

Abstract

The inclusive production of the $\omega(782)$ vector meson in hadronic Z decays is measured and compared to model predictions. The analysis is based on 4 million hadronic Z decays recorded by the ALEPH detector between 1991 and 1995. The production rate for $x_p = p_{\mathrm{meson}}/p_{\mathrm{beam}} > 0.05$ is measured in the $\omega \to \pi^+\pi^-\pi^0$ decay mode and found to be $0.585 \pm 0.019_{\mathrm{stat}} \pm 0.033_{\mathrm{sys}}$ per event. Inclusive η meson production is also measured in the same decay channel for $x_p > 0.10$, obtaining $0.355 \pm 0.011_{\mathrm{stat}} \pm 0.024_{\mathrm{sys}}$ per event. The branching ratio for $\omega \to \mu^+\mu^-$ is investigated. A total of 18.1 ± 5.9 events are observed, from which the muonic branching ratio is measured for the first time to be $\mathrm{BR}(\omega \to \mu^+\mu^-) = (9.0\pm2.9_{\mathrm{stat}}\pm1.1_{\mathrm{sys}})\times10^{-5}$.

To be submitted to Phys. Lett. B

*) See next pages for the list of authors

The ALEPH Collaboration

A. Heister, S. Schael

Physikalisches Institut das RWTH-Aachen, D-52056 Aachen, Germany

R. Barate, I. De Bonis, D. Decamp, C. Goy, J.-P. Lees, E. Merle, M.-N. Minard, B. Pietrzyk

Laboratoire de Physique des Particules (LAPP), IN^{2}P^3-CNRS, F-74019 Annecy-le-Vieux Cedex, France

G. Boix, S. Bravo, M.P. Casado, M. Chmeissani, J.M. Crespo, E. Fernandez, M. Fernandez-Bosman, Ll. Garrido,[15] E. Graugés, M. Martinez, G. Merino, R. Miquel,[27] Ll.M. Mir,[27] A. Pacheco, H. Ruiz

Institut de Fisica d'Altes Energies, Universitat Autònoma de Barcelona, E-08193 Bellaterra (Barcelona), Spain[7]

A. Colaleo, D. Creanza, M. de Palma, G. Iaselli, G. Maggi, M. Maggi, S. Nuzzo, A. Ranieri, G. Raso,[23] F. Ruggieri, G. Selvaggi, L. Silvestris, P. Tempesta, A. Tricomi,[3] G. Zito

Dipartimento di Fisica, INFN Sezione di Bari, I-70126 Bari, Italy

X. Huang, J. Lin, Q. Ouyang, T. Wang, Y. Xie, R. Xu, S. Xue, J. Zhang, L. Zhang, W. Zhao

Institute of High Energy Physics, Academia Sinica, Beijing, The People's Republic of China[8]

D. Abbaneo, P. Azzurri, O. Buchmüller,[25] M. Cattaneo, F. Cerutti, B. Clerbaux, H. Drevermann, R.W. Forty, M. Frank, F. Gianotti, T.C. Greening,[29] J.B. Hansen, J. Harvey, D.E. Hutchcroft, P. Janot, B. Jost, M. Kado,[27] P. Mato, A. Moutoussi, F. Ranjard, L. Rolandi, D. Schlatter, O. Schneider,[2] G. Sguazzoni, W. Tejessy, F. Teubert, A. Valassi, I. Videau, J. Ward

European Laboratory for Particle Physics (CERN), CH-1211 Geneva 23, Switzerland

F. Badaud, A. Falvard,[22] P. Gay, P. Henrard, J. Jousset, B. Michel, S. Monteil, J-C. Montret, D. Pallin, P. Perret

Laboratoire de Physique Corpusculaire, Université Blaise Pascal, IN^{2}P^3-CNRS, Clermont-Ferrand, F-63177 Aubière, France

J.D. Hansen, J.R. Hansen, P.H. Hansen, B.S. Nilsson, A. Wäänänen

Niels Bohr Institute, DK-2100 Copenhagen, Denmark[9]

A. Kyriakis, C. Markou, E. Simopoulou, A. Vayaki, K. Zachariadou

Nuclear Research Center Demokritos (NRCD), GR-15310 Attiki, Greece

A. Blondel,[12] G. Bonneaud, J.-C. Brient, A. Rougé, M. Rumpf, M. Swynghedauw, M. Verderi, H. Videau

Laboratoire de Physique Nucléaire et des Hautes Energies, Ecole Polytechnique, IN^{2}P^3-CNRS, F-91128 Palaiseau Cedex, France

V. Ciulli, E. Focardi, G. Parrini

Dipartimento di Fisica, Università di Firenze, INFN Sezione di Firenze, I-50125 Firenze, Italy

A. Antonelli, M. Antonelli, G. Bencivenni, G. Bologna,[4] F. Bossi, P. Campana, G. Capon, V. Chiarella, P. Laurelli, G. Mannocchi,[5] F. Murtas, G.P. Murtas, L. Passalacqua, M. Pepe-Altarelli,[24] P. Spagnolo

Laboratori Nazionali dell'INFN (LNF-INFN), I-00044 Frascati, Italy

A. Halley, J.G. Lynch, P. Negus, V. O'Shea, C. Raine,[4] A.S. Thompson

Department of Physics and Astronomy, University of Glasgow, Glasgow G12 8QQ, United Kingdom[10]

S. Wasserbaech

Department of Physics, Haverford College, Haverford, PA 19041-1392, U.S.A.

R. Cavanaugh, S. Dhamotharan, C. Geweniger, P. Hanke, G. Hansper, V. Hepp, E.E. Kluge, A. Putzer, J. Sommer, K. Tittel, S. Werner,[19] M. Wunsch[19]

Kirchhoff-Institut für Physik, Universität Heidelberg, D-69120 Heidelberg, Germany[16]

R. Beuselinck, D.M. Binnie, W. Cameron, P.J. Dornan, M. Girone,[1] N. Marinelli, J.K. Sedgbeer, J.C. Thompson[14]

Department of Physics, Imperial College, London SW7 2BZ, United Kingdom[10]

V.M. Ghete, P. Girtler, E. Kneringer, D. Kuhn, G. Rudolph

Institut für Experimentalphysik, Universität Innsbruck, A-6020 Innsbruck, Austria[18]

E. Bouhova-Thacker, C.K. Bowdery, A.J. Finch, F. Foster, G. Hughes, R.W.L. Jones, M.R. Pearson, N.A. Robertson

Department of Physics, University of Lancaster, Lancaster LA1 4YB, United Kingdom[10]

K. Jakobs, K. Kleinknecht, G. Quast,[6] B. Renk, H.-G. Sander, H. Wachsmuth, C. Zeitnitz

Institut für Physik, Universität Mainz, D-55099 Mainz, Germany[16]

A. Bonissent, J. Carr, P. Coyle, O. Leroy, P. Payre, D. Rousseau, M. Talby

Centre de Physique des Particules, Université de la Méditerranée, IN²P³-CNRS, F-13288 Marseille, France

F. Ragusa

Dipartimento di Fisica, Università di Milano e INFN Sezione di Milano, I-20133 Milano, Italy

A. David, H. Dietl, G. Ganis,[26] K. Hüttmann, G. Lütjens, C. Mannert, W. Männer, H.-G. Moser, R. Settles, H. Stenzel, W. Wiedenmann, G. Wolf

Max-Planck-Institut für Physik, Werner-Heisenberg-Institut, D-80805 München, Germany[16]

J. Boucrot, O. Callot, M. Davier, L. Duflot, J.-F. Grivaz, Ph. Heusse, A. Jacholkowska,[22] J. Lefrançois, J.-J. Veillet, C. Yuan

Laboratoire de l'Accélérateur Linéaire, Université de Paris-Sud, IN²P³-CNRS, F-91898 Orsay Cedex, France

G. Bagliesi, T. Boccali, L. Foà, A. Giammanco, A. Giassi, F. Ligabue, A. Messineo, F. Palla, G. Sanguinetti, A. Sciabà, R. Tenchini,[1] A. Venturi,[1] P.G. Verdini

Dipartimento di Fisica dell'Università, INFN Sezione di Pisa, e Scuola Normale Superiore, I-56010 Pisa, Italy

G.A. Blair, G. Cowan, M.G. Green, T. Medcalf, A. Misiejuk, J.A. Strong, P. Teixeira-Dias, J.H. von Wimmersperg-Toeller

Department of Physics, Royal Holloway & Bedford New College, University of London, Egham, Surrey TW20 OEX, United Kingdom[10]

R.W. Clifft, T.R. Edgecock, P.R. Norton, I.R. Tomalin

Particle Physics Dept., Rutherford Appleton Laboratory, Chilton, Didcot, Oxon OX11 OQX, United Kingdom[10]

B. Bloch-Devaux, P. Colas, S. Emery, W. Kozanecki, E. Lançon, M.-C. Lemaire, E. Locci, P. Perez, J. Rander, J.-F. Renardy, A. Roussarie, J.-P. Schuller, J. Schwindling, A. Trabelsi,[21] B. Vallage

CEA, DAPNIA/Service de Physique des Particules, CE-Saclay, F-91191 Gif-sur-Yvette Cedex, France[17]

N. Konstantinidis, A.M. Litke, G. Taylor

Institute for Particle Physics, University of California at Santa Cruz, Santa Cruz, CA 95064, USA[13]

A. Beddall,[30] C.N. Booth, S. Cartwright, F. Combley,[4] M. Lehto, L.F. Thompson

Department of Physics, University of Sheffield, Sheffield S3 7RH, United Kingdom[10]

K. Affholderbach,[28] A. Böhrer, S. Brandt, C. Grupen, A. Ngac, G. Prange, U. Sieler

Fachbereich Physik, Universität Siegen, D-57068 Siegen, Germany[16]

G. Giannini

Dipartimento di Fisica, Università di Trieste e INFN Sezione di Trieste, I-34127 Trieste, Italy

J. Rothberg

Experimental Elementary Particle Physics, University of Washington, Seattle, WA 98195 U.S.A.

S.R. Armstrong, K. Berkelman, K. Cranmer, D.P.S. Ferguson, Y. Gao,[20] S. González, O.J. Hayes, H. Hu, S. Jin, J. Kile, P.A. McNamara III, J. Nielsen, Y.B. Pan, J.H. von Wimmersperg-Toeller, W. Wiedenmann, J. Wu, Sau Lan Wu, X. Wu, G. Zobernig

Department of Physics, University of Wisconsin, Madison, WI 53706, USA[11]

G. Dissertori

Institute for Particle Physics, ETH Hönggerberg, 8093 Zürich, Switzerland.

1 Introduction

The description of the hadronization process in QCD is deeply connected with the confinement property and requires non-perturbative methods. The precise measurement of momentum spectra of identified particles in the clean environment of e^+e^- annihilation into hadrons may improve the understanding of hadronization. Meanwhile these measurements are necessary to test and tune the phenomenological models used to describe the hadronization: each of these models has free parameters which must be determined from comparison with data [1].

Resonant states and their dynamics are more closely related to the original partons than pions. The η and $\omega(782)$ mesons are copiously produced in hadronic events and thus well suited to a study of hadronization.

In this investigation a measurement of the inclusive momentum distributions of the η and ω mesons obtained through their $\pi^+\pi^-\pi^0$ decays is presented, which improves on the previous ALEPH results [2] with higher statistics and reduced systematic effects. It also complements the recent publication concerning the $\gamma\gamma$ decay of the η meson [3]. Studies by the OPAL and L3 Collaborations can be found in [4, 5, 6].

The measurement of the partial width of leptonic decay rates of the light vector mesons is a good test both for the quark assignments ($\sum a_q q\bar{q}$ with $q = \mathrm{u, d, s}$) in the vector meson and the quark charges. With $\rho^0 = (\mathrm{u\bar{u} - d\bar{d}})/\sqrt{2}$, $\omega = (\mathrm{u\bar{u} + d\bar{d}})/\sqrt{2}$ and $\phi = \mathrm{s\bar{s}}$ the partial decay width of a vector meson V to lepton pairs ($\ell = e^\pm, \mu^\pm$) can be calculated using the Van Royen-Weisskopf formula [7]:

$$\Gamma_\ell(\mathrm{V} \to \ell^+\ell^-) = \frac{16\pi\alpha^2 Q^2}{m_\mathrm{V}^2}|\psi(0)|^2 ,$$

where $Q^2 = (\sum a_q Q_q)^2$ is the square of the flavour-weighted sum of the charges Q_q of the quarks ($q = \mathrm{u, d, s}$), $\psi(0)$ is the amplitude of the $\mathrm{q\bar{q}}$ wavefunction at the origin, and m_V is the meson mass. The expected ratio of the leptonic widths is $\Gamma_\ell(\rho^0) : \Gamma_\ell(\omega) : \Gamma_\ell(\phi) = 9 : 1 : 2$ in agreement with the widths and branching ratios measured as summarized in [8] for the decay to e^+e^-. While $\Gamma_\ell(\rho^0)$ and $\Gamma_\ell(\phi)$ are in agreement with the prediction based on the Van Royen-Weisskopf formula and lepton universality also for the muonic decay, only an upper limit [8] so far has been established for the decay $\omega \to \mu^+\mu^-$ (Table 1). The muonic branching ratio of the ω is measured here for the first time.

Table 1: Widths and leptonic branching ratios of the light vector mesons V [8]

	Γ [MeV]	BR(V $\to e^+e^-$)	BR(V $\to \mu^+\mu^-$)
ρ^0	150.2±0.8	$(4.49 \pm 0.22) \times 10^{-5}$	$(4.60 \pm 0.28) \times 10^{-5}$
ω	8.44±0.09	$(7.07 \pm 0.19) \times 10^{-5}$	(CL=90%) $< 1.8 \times 10^{-4}$
ϕ	4.46±0.03	$(2.91 \pm 0.07) \times 10^{-4}$	$(3.7 \pm 0.5) \times 10^{-4}$

After a brief description of the ALEPH detector, the selection of hadronic events is detailed in Section 3 and the particle identification in Section 4. The improved measurement of inclusive η and ω production in the $\pi^+\pi^-\pi^0$ channel with a large data sample of about 4 million hadronic Z decays is presented in Section 5. The measurement of the branching ratio $\omega \to \mu^+\mu^-$ is presented in Section 6, followed by a summary and conclusions.

2   The ALEPH Detector

The ALEPH detector is described in detail elsewhere [9, 10]. Charged particles are measured over the polar angle range $|\cos\theta| < 0.85$ and $|\cos\theta| < 0.69$ by the two layers of the silicon vertex detector (VDET). This is surrounded by a cylindrical inner drift chamber, and a large cylindrical time projection chamber (TPC) which measures up to 21 three-dimensional space points per track. A particle's energy loss is sampled in the TPC by up to 338 wires and 21 pads. The tracking detectors are immersed in a magnetic field of 1.5 T and provide a momentum resolution of $\delta p_t/p_t = 0.0006 p_t \oplus 0.005$ (p_t in GeV/c). The TPC is surrounded by an electromagnetic calorimeter (ECAL) of lead-proportional tube construction, which covers the angular range $|\cos\theta| < 0.98$ and has a thickness of 22 radiation lengths. It is finely segmented in projective towers of approximately $0.9°$ by $0.9°$ providing an angular resolution of $\sigma_{\theta,\phi} = 2.5/\sqrt{E} + 0.25$ (E in GeV; $\sigma_{\theta,\phi}$ in mrad). The energy resolution is $\sigma_E/E = 0.18/\sqrt{E} + 0.009$ (E in GeV) for isolated showers. The hadron calorimeter (HCAL) uses the iron return yoke as an absorber, for a total of 7.5 hadronic interaction lengths. The iron is interleaved by 23 layers of streamer tubes, which provide a two-dimensional measurement of muon tracks and a view of the hadronic shower development. The HCAL is used in conjunction with the muon chambers, which are two double-layers of streamer tubes with three-dimensional readout, and the tracking detectors to identify muons. The calorimeters and the muon chambers cover nearly the entire 4π solid angle.

3   Event Selection

For the event selection, good tracks are defined as originating close to the interaction point (with transverse impact parameter $|d_0| < 2$ cm and longitudinal impact parameter $|z_0| < 5$ cm), having at least 4 TPC hits, a polar angle in the range $20° < \theta < 160°$, and a transverse momentum $p_t > 200$ MeV/c. Four million hadronic Z decays are selected by requiring at least five good tracks. The total energy carried by all good tracks is required to exceed 15 GeV and the sphericity axis must be in the range $35° < \theta < 145°$. With these cuts, a sample of 3.0 million events is selected. The background to these events arises from tau pairs and two-photon events and is estimated to be less than 0.4% [11].

For the measurement of the branching ratio BR($\omega \to \mu^+\mu^-$) additional event cuts are applied to reject heavy flavour events and events with missing energy: events from $Z \to b\bar{b}$ and $Z \to c\bar{c}$ are rejected by a lifetime tag [12] keeping about 95% of light flavours. A further reduction is obtained by a cut on the missing energy corrected with hemisphere masses [13], $E_{\mathrm{miss}} < 6$ GeV, in the ω hemisphere.

For the purpose of comparing with models and as a means of measuring the detector acceptance, samples of events generated with the JETSET 7.4 Monte Carlo [14], modified with DYMU3 [15] for electromagnetic radiative effects and improved bottom and charm decay tables, were passed through a full detector simulation and reconstruction program. The generator was tuned to describe the ALEPH data using the inclusive charged particle and event shape distributions [16]. For model comparison and as a systematic check for the extrapolation into the unmeasured region the measured spectra were compared to those of HERWIG 5.9 [17]. The model parameters were tuned using ALEPH data in the same manner as mentioned above. For the measurement of the branching ratio BR($\omega \to \mu^+\mu^-$) a sample of events was generated with the JETSET 7.4 Monte Carlo, but with the muonic branching ratio of the ω meson BR($\omega \to \mu^+\mu^-$) set to 100%. After a full

detector simulation and reconstruction, the generated events were subjected to the same selection and analysis chain as the data.

4 Particle Identification

The η and ω mesons are produced and decay at or near the primary interaction point. To reduce background from charged particles produced far from the interaction point, e.g., from K_S^0 decays or photon conversions, track candidates are required to be reconstructed as good tracks (as discussed above) with tighter cuts on the impact parameters ($|d_0| < 0.5$ cm and $|z_0| < 3.0$ cm) and the transverse momentum ($p_t > 250$ MeV$/c$).

For the measurement of the branching ratio BR($\omega \rightarrow \mu^+\mu^-$) additional cuts are applied to identify and select muons above the background of mainly charged pions. One VDET hit is required. For the identification of muons the measured energy loss in the TPC, dE/dx_{meas} should be consistent with the expectation for a muon, $(dE/dx_{meas} - dE/dx_{exp})/\sigma_{exp} > -2$, where dE/dx_{exp} and σ_{exp} are the expected energy loss and its resolution. The pattern in HCAL and the muon chambers should match with the pattern expected for penetrating muons, if the momentum is larger than 2.4 GeV$/c$. For lower momenta, 1.5 GeV$/c < p < 2.4$ GeV$/c$, the number of fired planes within the last ten HCAL planes divided by the number of all fired planes should be between 0.35 and 0.75 [18, 19].

For the selection of neutral pions two-photon invariant mass spectra are formed. The photon energy is estimated from the energy collected in the four central ECAL towers of a cluster, correcting to the full energy from a parametrization of the shower shape for a single photon in the calorimeter. While the energy resolution is degraded to $\sigma_E/E \approx 0.25/\sqrt{E}$ (E in GeV) with this technique, hadronic background and clustering effects are reduced. Photon candidates are only accepted if the estimated energy is greater than 0.8 GeV. Neutral pion candidates are accepted if the energy of the photon pair is less than 16 GeV (to remove large uncertainties in the acceptance correction at high energy). The invariant mass of the photon pair must also be within $\pm 3\sigma$ of the expected mass. The π^0 energy resolution is improved by constraining the mass of the π^0 candidates to 135 MeV$/c^2$. The poor purity at low momentum, due to the large multiplicity of low energy photons giving rise to a large combinatorial background, is improved by a "ranking" method: candidates that share photons with other candidates are ranked in an order determined by a π^0 estimator. The estimator R is calculated for each candidate from the photon pair opening angle θ_{12} and the χ^2 from the mass constraint:

$$R = \theta_{12}(1.0 + 0.1\chi^2).\tag{1}$$

All π^0 candidates sharing photons with other candidates are removed except the one with the smallest value of R.

5 Inclusive Production of η and ω

5.1 Extraction of the η and ω Signals

The η and ω cross sections are extracted from invariant mass distributions in the $\pi^+\pi^-\pi^0$ decay mode. All charged tracks are assigned the charged pion mass; for neutral pion candidates the kinematic refit constrains the mass to the π^0 mass. Data are analysed in six intervals of scaled momentum $x_p = p_{meson}/p_{beam}$, where p_{beam} is the LEP beam
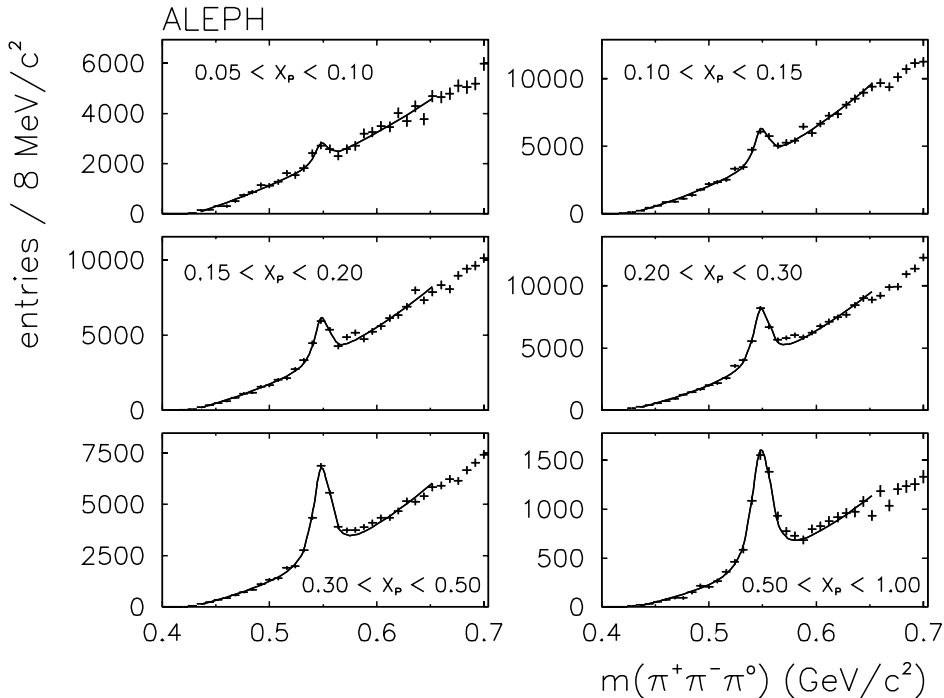
3

Figure 1: Fits in the η region made to the invariant mass spectra of data (like-sign subtracted).

momentum. Only candidates satisfying $x_p > 0.10$ for the η and $x_p > 0.05$ for the ω are considered, as the signal to background ratio is too small for lower momenta.

The invariant mass spectra are fitted as the sum of a background and a signal function. Subtracting the like-sign spectra from the unlike-sign spectra allows the backgrounds to be represented simply by a third order polynomial. The signal function is empirically parametrized as the sum of three Gaussian functions; the relative widths and normalizations of the three Gaussians are determined from the Monte Carlo and are fixed with the overall normalization left free. The results of fits to the data for the η and ω are shown in Figs. 1 and 2, respectively. The fit to the first momentum interval for the η yields a large ($\approx 50\%$) uncertainty, therefore this momentum interval is not considered further.

5.2 Measured Rates and Differential Cross-Section

The production rate per event, R, is calculated for each momentum interval by correcting the fitted signal S for the reconstruction efficiency ε and normalizing to one event. The rate is corrected for the branching ratio $\mathrm{BR}(\eta \rightarrow \pi^+\pi^-\pi^0) = 0.230 \pm 0.004$, $\mathrm{BR}(\omega \rightarrow \pi^+\pi^-\pi^0) = 0.888 \pm 0.007$, and $\mathrm{BR}(\pi^0 \rightarrow \gamma\gamma) = 0.9880 \pm 0.0003$ [8] to give the rate for all decay modes. The calculation is as follows:

$$R = \frac{S}{N} \frac{1}{\varepsilon} \frac{1}{\mathrm{BR}} \tag{2}$$

where N is the total number of hadronic events in data and ε is the efficiency. N is obtained as $N = N_{\mathrm{gen}} \cdot N_{\mathrm{acc}}^{\mathrm{d}} / N_{\mathrm{acc}}^{\mathrm{MC}}$, where N_{gen} is the number of generated events in the Monte Carlo, while $N_{\mathrm{acc}}^{\mathrm{d}}$ and $N_{\mathrm{acc}}^{\mathrm{MC}}$ are the numbers of accepted events after preselection in data and Monte Carlo, respectively. The efficiency ε is defined as $\varepsilon = n_{\mathrm{rec}}/n_{\mathrm{gen}}$, where n_{rec} is the number of reconstructed η (ω) mesons in the Monte Carlo, and n_{gen} is the number of generated η (ω) mesons in the Monte Carlo (before event selection cuts).
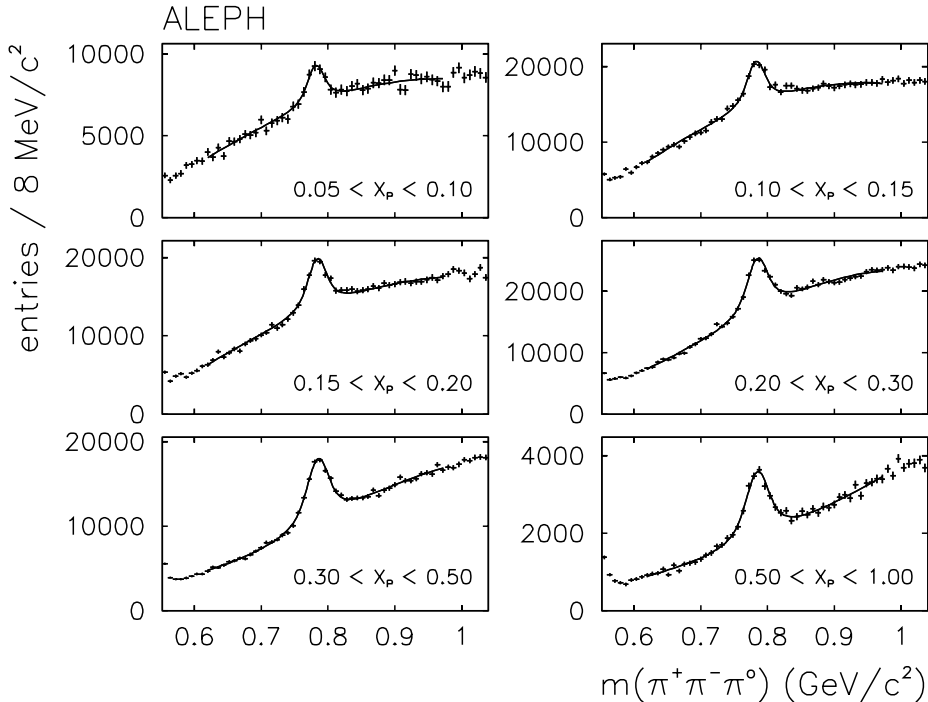
Figure 2: Fits in the ω region made to the invariant mass spectra of data (like-sign subtracted).

The implementation of the $\eta \to \pi^+\pi^-\pi^0$ decay in JETSET is according to phase space, while for the $\omega \to \pi^+\pi^-\pi^0$ decay it is according to the correct matrix element. For this analysis the Monte Carlo was reweighted for the η decay by parametrizing the decay transition probability λ_η as $\lambda_\eta \propto 1 - T_0^*/T_{0,\mathrm{max}}^*$ as suggested in [4], where T_0^* is the kinetic energy of the neutral pion in the η rest frame and $T_{0,\mathrm{max}}^*$ is its maximum possible value. This form is consistent with $\lambda_\eta \propto 1 + 2\alpha y$ proposed in [20] and the measurements in [20, 21], where $y = (3T_0^*/Q) - 1$, Q is the mass difference between the η and its daughters, and $\alpha = -0.47 \pm 0.04$. The η efficiency is taken as the average of the results obtained with the two parametrizations.

The overall efficiency in the measured momentum region is 15.3% for the η and 11.2% for the ω. The measurements cover only the momentum region $x_p > 0.10$ for the η and $x_p > 0.05$ for the ω. To estimate the total production rate the measured rates are extrapolated to $x_p = 0$ using the fragmentation function in the Monte Carlo. The fraction of η mesons for $x_p > 0.10$ is 29.56%. For the ω meson the fraction for $x_p > 0.05$ is 58.8%.

5.3   Systematic Uncertainties

The largest systematic uncertainties are determined to stem from the photon energy cut, the impact parameter cut, fit range and signal width, description of the neutral pion spectrum, and the uncertainty in the η and ω branching ratios. Systematic uncertainties are determined by varying cuts and taking the largest change in the calculated rate as the systematic error. Additionally, a systematic error is assigned representing the uncertainty in the extrapolation of the measured rate to $x_p = 0$. Details of the systematic checks are given below.

A cut of 0.8 GeV is applied on the energy of photons. This cut is varied by ± 0.1 GeV. A d_0 cut of 0.5 cm is applied to remove tracks originating from decays of particles at some distance away from the primary interaction point. As this cut is tight a check

5

is performed to determine any associated systematic uncertainty. This cut is decreased to 0.3 cm and increased to 1.0 cm. Other cuts on charged track parameters do not have significant systematic uncertainties associated with them.

In the fitting procedure mass spectra are fitted six times with a different fit range. The value for the extracted signal is seen to vary; a systematic error is assigned to this, calculated as the standard deviation of the six results. For the η, significant variations in extracted signals occur for different choices of the background function, and a systematic error is assigned for this fitting uncertainty. The fitting procedure is repeated with the width of the signal function as a free parameter, and the variation in the number of extracted mesons is taken as a systematic error. To check the effect of fixing the mass in the fitting procedure, the procedure is repeated with the mass as a free parameter in the fit. The fitted masses are found to be stable and no significant variation in the extracted number of mesons was found, therefore no systematic error is assigned. Uncertainties in the meson reconstruction efficiency arise from the modelling of the π^0 spectrum. It has been checked that bin-to-bin migration effects are below 1% for all but the highest x_p bin. Even there the estimated effect is smaller than other relevant systematic uncertainties.

For the η, the effect of the matrix element proposed by [4] and [20] which is not included in JETSET is corrected for by reweighting JETSET to agree with proposed parametrizations. Although little effect on the momentum spectra is seen for high η momenta, the effect at low momenta is large (23% in the lowest measured momentum interval). As a correction, the mean of the two weighting schemes is applied to the measured rates, and the difference in the two schemes in each momentum interval is taken as the systematic error.

Statistical and systematic errors are summarized in Tables 2 and 3 for the η and ω measurements, respectively. For the systematic errors the individual errors from each source are shown for each measured momentum interval (1 to 6). The error for the total measured momentum range, calculated for each error source, is taken as the sum of the errors in each interval weighted by the rate in each interval. The calculations take into consideration whether the errors are correlated or not. The statistical errors are taken from the fitting procedure. The last line shows the final error for each momentum interval.

The extrapolation of the measured rates to $x_p = 0$ relies on the Monte Carlo to give the correct scale factor for the extrapolation. For the extrapolation the shape of the fragmentation function in JETSET 7.4 is used. To estimate the uncertainty in the scale factor the calculation is repeated for the HERWIG Monte Carlo. For the η, extrapolating from $x_p = 0.10$, the difference, 5.8%, between HERWIG 5.9 and JETSET 7.4 is taken as the systematic uncertainty in the extrapolation. For the ω, extrapolating from $x_p = 0.05$, the difference, 2.4%, between HERWIG 5.9 and JETSET 7.4 is taken as the systematic uncertainty in the extrapolation.

5.4   Results

Table 4 shows the results for rates and differential cross sections in each measured momentum interval. Results of summing over the measured x_p intervals are shown; the final line gives the result of extrapolating this to $x_p = 0$ together with an extra error of 5.8% and 2.4% representing the uncertainty in the extrapolation of the measured η and ω rates, respectively. Measured differential cross sections are compared to Monte Carlo predictions in Figs. 3 and 4 for the η and ω, respectively. Table 5 compares the total rate in the data to the Monte Carlo predictions. The errors are the quadratic sum of the statistical and systematic contributions. The final column gives the result of extrapolating

Table 2: Systematic and statistical errors on the η production rate in each measured momentum interval. All values are expressed in percent.

Source of error (η)	measured x_p interval						
	all	1	2	3	4	5	6
Photon energy cut	4.5	-	12.1	6.7	3.4	1.2	1.4
Track selection	1.1	-	2.5	3.2	0.4	1.7	1.7
Fit range and background	2.0	-	5.0	3.3	3.0	1.4	2.0
Fit width	1.5	-	3.2	4.5	0.4	2.6	1.4
π^0 spectrum	2.8	-	2.8	2.8	2.5	2.9	4.8
η branching ratio	2.2	-	2.2	2.2	2.2	2.2	2.2
η matrix element	2.3	-	3.9	2.2	1.4	1.1	0.3
Total systematic error	6.8	-	14.7	10.2	5.8	5.2	6.2
Statistical error	3.1	-	7.9	5.6	3.5	2.3	3.0
Total error	7.5	-	16.7	11.6	6.8	5.7	6.9

Table 3: Systematic and statistical errors on the ω production rate in each measured momentum interval. All values are expressed in percent.

Source of error (ω)	measured x_p interval						
	all	1	2	3	4	5	6
Photon energy cut	4.1	10.6	2.2	2.8	1.7	0.1	1.8
Track selection	2.6	6.7	1.9	1.2	1.1	0.5	1.1
Fit range	1.0	1.7	3.2	2.2	2.0	0.3	1.1
Fit width	0.8	1.0	3.3	1.8	0.4	0.2	0.5
π^0 spectrum	2.7	2.5	2.8	2.8	2.5	2.9	4.8
ω branching ratio	0.7	0.7	0.7	0.7	0.7	0.7	0.7
Total systematic error	5.7	13.0	6.2	5.1	3.9	3.0	5.4
Statistical error	3.2	7.8	4.2	3.3	2.8	2.0	2.9
Total error	6.5	15.2	7.5	6.1	4.8	3.6	6.1

the measured rate to $x_p = 0$. Values inside the brackets indicate the discrepancy between Monte Carlo and data in terms of the total experimental error. Table 6 compares the results of the η measurement with results published by ALEPH [3], OPAL [4] and L3 [5]. For the ω, Table 7 compares the results with those of published results by ALEPH [2], OPAL [4] and L3 [6].

For the η, the total estimated production rate of $1.200 \pm 0.037_{\text{stat}} \pm 0.082_{\text{sys}} \pm 0.070_{\text{extrap}}$ per event is somewhat higher than the predictions of both JETSET 7.4 (1.00 η per event) and HERWIG 5.9 (1.04 η per event). This result is also somewhat higher than the results published by LEP experiments. The two measurements for the $\eta \rightarrow \gamma\gamma$ mode [3] and the $\eta \rightarrow \pi^+\pi^-\pi^0$ mode differ by more than twice the estimated error, the ratio (rate obtained with the $\pi^+\pi^-\pi^0$ mode to the rate obtained with the $\gamma\gamma$ mode) being $1.26 \pm 0.04_{\text{stat}} \pm 0.10_{\text{sys}}$. This is consistent with a recent finding by OPAL [4] of $1.14 \pm 0.07_{\text{stat}} \pm 0.13_{\text{sys}}$ for the same ratio.

For the ω, the total estimated production rate of $0.996 \pm 0.032_{\text{stat}} \pm 0.057_{\text{sys}} \pm 0.024_{\text{extrap}}$ per event lies significantly below the prediction of JETSET 7.4 (1.31 ω per event) and

Table 4: Measured production rates per hadronic event and differential cross sections for the η and ω. The errors correspond to statistical and systematic uncertainties. The value for the total systematic error is taken from Table 2 and Table 3 for the η and ω respectively, where correlations between errors are taken into account. The results of summing over the measured x_p intervals are given, including the extrapolation to the full x_p range with an additional error representing the uncertainty in the extrapolation.

x_p	η rate	$1/\sigma_{\mathrm{tot}} \cdot d\sigma/dx_p$
0.10-0.15	$0.1236 \pm 0.0098 \pm 0.0182$	$2.471 \pm 0.195 \pm 0.363$
0.15-0.20	$0.0753 \pm 0.0042 \pm 0.0077$	$1.506 \pm 0.084 \pm 0.154$
0.20-0.30	$0.0802 \pm 0.0028 \pm 0.0047$	$0.802 \pm 0.028 \pm 0.047$
0.30-0.50	$0.0611 \pm 0.0014 \pm 0.0032$	$0.306 \pm 0.007 \pm 0.016$
0.50-1.00	$0.0146 \pm 0.0004 \pm 0.0009$	$0.029 \pm 0.001 \pm 0.002$
0.10-1.00	$0.355 \ \pm 0.011 \ \ \ \pm 0.024$	
all	$1.200 \ \pm 0.037 \ \ \ \pm 0.082 \pm 0.070$	

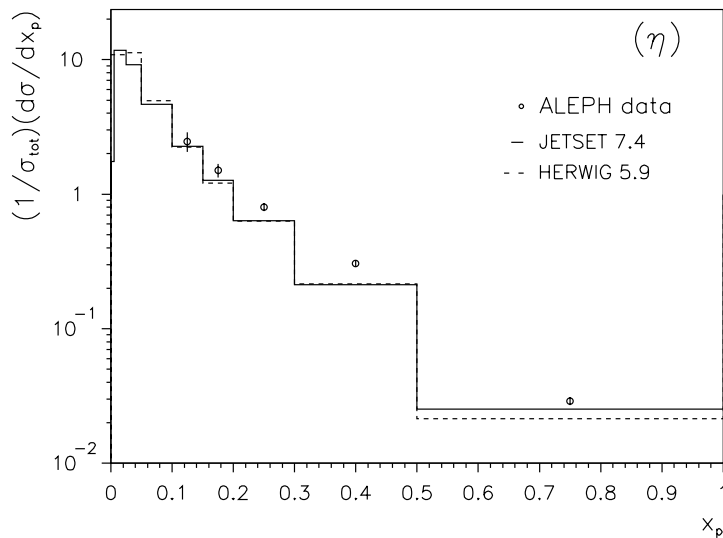| x_p	ω rate	$1/\sigma_{\mathrm{tot}} \cdot d\sigma/dx_p$
0.05-0.10	$0.2222 \pm 0.0173 \pm 0.0289$	$4.444 \pm 0.347 \pm 0.578$
0.10-0.15	$0.1246 \pm 0.0052 \pm 0.0065$	$2.493 \pm 0.105 \pm 0.130$
0.15-0.20	$0.0825 \pm 0.0027 \pm 0.0042$	$1.650 \pm 0.054 \pm 0.084$
0.20-0.30	$0.0852 \pm 0.0024 \pm 0.0033$	$0.852 \pm 0.024 \pm 0.033$
0.30-0.50	$0.0569 \pm 0.0011 \pm 0.0017$	$0.284 \pm 0.006 \pm 0.009$
0.50-1.00	$0.0139 \pm 0.0004 \pm 0.0008$	$0.028 \pm 0.001 \pm 0.002$
0.05-1.00	$0.585 \ \pm 0.019 \ \ \ \pm 0.033$	
all	$0.996 \ \pm 0.032 \ \ \ \pm 0.057 \pm 0.024$	

Figure 3: Measured differential cross sections for the η in comparison with Monte Carlo predictions. The errors shown are the quadratic sum of statistical and systematic contributions.
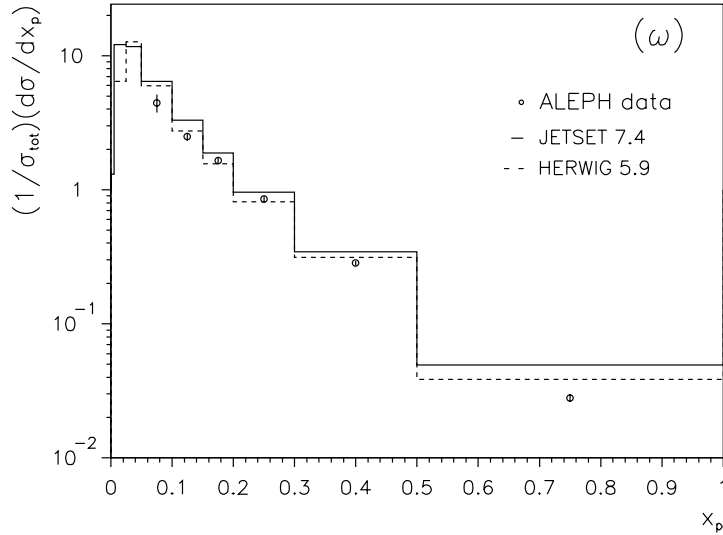
8

Figure 4: Measured differential cross sections for the ω in comparison with Monte Carlo predictions. The errors shown are the quadratic sum of statistical and systematic contributions.

Table 5: Comparison of the total measured production rates with Monte Carlo predictions. Values in parentheses indicate the discrepancy between Monte Carlo and data in terms of the total experimental error.

	$(\eta)\ x_p > 0.10$	(η) all x_p
data	0.355 ± 0.026	1.20 ± 0.11
JETSET 7.4	$0.296\ (-2.3\sigma)$	$1.00\ (-1.8\sigma)$
HERWIG 5.9	$0.289\ (-2.5\sigma)$	$1.04\ (-1.5\sigma)$

	$(\omega)\ x_p > 0.05$	(ω) all x_p
data	0.585 ± 0.038	0.996 ± 0.070
JETSET 7.4	$0.771\ (+4.9\sigma)$	$1.310\ (+4.5\sigma)$
HERWIG 5.9	$0.678\ (+2.4\sigma)$	$1.125\ (+1.8\sigma)$

Table 6: η rate measured in this analysis compared to values published by LEP experiments.

Experiment	η decay mode	η rate
L3 [5]	$\gamma\gamma$	$0.93 \pm 0.01 \pm 0.09 \pm 0.06$
OPAL [4]	$\gamma\gamma,\ \pi^+\pi^-\pi^0$	$0.97 \pm 0.03 \pm 0.10 \pm 0.04$
this study	$\pi^+\pi^-\pi^0$	$1.20 \pm 0.04 \pm 0.08 \pm 0.07$
ALEPH [3] $x_p > 0.10$	$\gamma\gamma$	$0.282 \pm 0.006 \pm 0.015$
this study $x_p > 0.10$	$\pi^+\pi^-\pi^0$	$0.355 \pm 0.011 \pm 0.024$

Table 7: Results for the ω production rate measured by three LEP experiments.

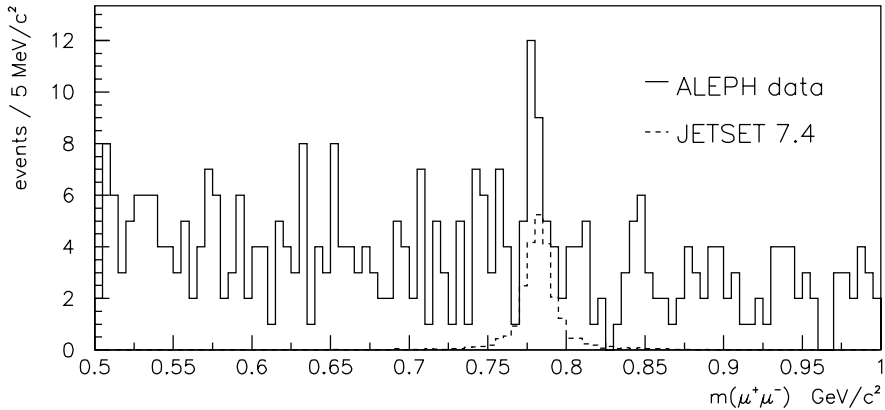| Experiment	ω rate
ALEPH [2]	$1.07 \pm 0.06 \pm 0.12 \pm 0.04$
L3 [6]	$1.17 \pm 0.09 \pm 0.15$
OPAL [4]	$1.04 \pm 0.04 \pm 0.13 \pm 0.03$
this study	$1.00 \pm 0.03 \pm 0.06 \pm 0.02$

Figure 5: Invariant mass distribution $m(\mu^+\mu^-)$ for hadronic events containing a muon pair after standard cuts as described in the text. The ω signal of JETSET is normalized to the signal in the data shown.
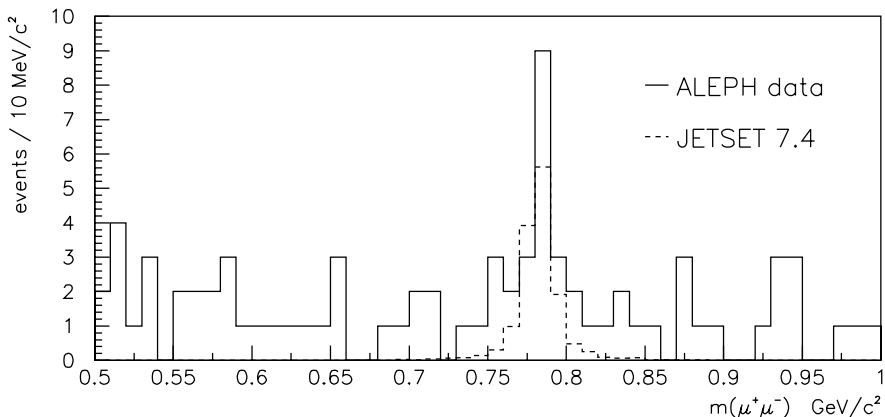

Figure 6: Invariant mass distribution $m(\mu^+\mu^-)$ for hadronic events containing a muon pair with tighter cuts (as explained in the text). The ω signal of JETSET is normalized to the signal in the data shown.

somewhat below that of HERWIG 5.9 (1.13 ω per event). Published results from L3 and OPAL for the production rate of the ω are in good agreement with the result of this analysis.

6   The Branching Ratio BR($\omega \to \mu^+\mu^-$)

6.1   Extraction of the Signal

The signal $\omega \to \mu^+\mu^-$ is obtained from the invariant mass distribution of two identified muons of opposite charge originating from a common vertex (Fig. 5). The signal is taken as the number of events in the mass region $770\,\mathrm{MeV}/c^2 < m(\mu^+\mu^-) < 795\,\mathrm{MeV}/c^2$ reduced by the estimated background in the same region. Monte Carlo studies have shown the background to be linear as a function of the invariant mass. The level of background in the signal region is extrapolated from the background in the sidebands in the mass ranges $500\,\mathrm{MeV}/c^2 < m(\mu^+\mu^-) < 745\,\mathrm{MeV}/c^2$ and $820\,\mathrm{MeV}/c^2 < m(\mu^+\mu^-) < 1000\,\mathrm{MeV}/c^2$. Applying the cuts described in Sections 3 and 4 results in an optimal signal-to-background ratio, $S/\sqrt{S+B}$.

6.2 Measurement of BR($\omega \rightarrow \mu^+\mu^-$)

Figure 5 shows 35 events in the signal region. A background of 16.94 events is estimated from the sidebands, leaving 18.06 ± 5.92 signal events. When the acceptance is taken from JETSET 7.4, but with the momentum spectrum and rate corrected to agree with the $\pi^+\pi^-\pi^0$ analysis, a muonic branching ratio BR($\omega \rightarrow \mu^+\mu^-$) = $(9.0 \pm 2.9) \times 10^{-5}$ is obtained, based on the selected events shown in Fig. 5.

The effect of tightening cuts in order to increase $S/\sqrt{B}$ is shown in Fig. 6. For this, the additional requirements are muon momenta greater than $2.5\,\mathrm{GeV}/c$, two VDET hits instead of one, and a stronger b$\bar{\text{b}}$ event rejection (keeping 90% of light quark-antiquark events). In the signal region 14 events are kept, with an estimated background of 3.24 events, leaving 10.76 ± 3.74 signal events.

6.3 Systematic Error Analysis

Uncertainties on the muonic branching ratio come from the uncertainty of the momentum spectrum of the ω and its rate in hadronic events, which are taken from the $\pi^+\pi^-\pi^0$ analysis. If the momentum spectrum from JETSET 7.4 is used, the extracted branching ratio would increase. Half of the difference from the shape of the spectrum is taken as systematic error (4%). Further systematic errors come from the uncertainty of the measured rate of ω production per event in the $\omega \rightarrow \pi^+\pi^-\pi^0$ analysis. Because event selection and track selection are similar in both analyses their errors are assumed fully correlated and neglected. The remaining errors (π^0 selection, fitting procedure, etc.) are studied by varying the Monte Carlo momentum spectrum according to these remaining errors. An error of 6% is obtained.

Possible uncertainties can arise from the track selection and b-tag probability. The last also changes the flavour composition of the sample; the ω rate for different flavours has not yet been measured. The $\pi^+\pi^-\pi^0$ analysis was therefore repeated with the cuts on b-tag probability and track selection from this analysis. An error of 4% is derived. The estimation of the background is dominated by the limited statistics in the sidebands. Smaller uncertainties come from a possible curvature of the background shape, e.g., due to the ρ meson. The error is determined to be 6%. Further systematic uncertainties are related to the performance of the ALEPH detector [10]: muon identification [19] (± 5%), tracking resolution, which influences the signal shape (± 5%), and the missing energy, the impact of which is found to be negligible. The limited Monte Carlo statistics adds 3% to the error. Other sources of systematic error such as background are found to be small and are neglected. The total systematic error is obtained by adding the contributions in quadrature, giving ± 13%.

6.4 Results

The muonic branching ratio is measured to be BR($\omega \rightarrow \mu^+\mu^-$) = $(9.0 \pm 2.9 \pm 1.1) \times 10^{-5}$ from the observation of 18.06 ± 5.92 signal events. This is in agreement with the expectation from the flavour composition of the vector mesons and from lepton universality.

7   Summary and Conclusion

The inclusive production of the η meson and the ω vector meson in hadronic Z decays has been studied and compared to model predictions. Decays of the type $\eta \to \pi^+\pi^-\pi^0$ are reconstructed for the momentum interval of $x_p > 0.10$ where $x_p = p_{\text{meson}}/p_{\text{beam}}$. Decays of the type $\omega \to \pi^+\pi^-\pi^0$ are reconstructed for the momentum interval of $x_p > 0.05$. A signal is seen in the muonic decay $\omega \to \mu^+\mu^-$.

The average η rate per event for $x_p > 0.10$ is measured to be $0.355\pm0.011_{\text{stat}}\pm0.024_{\text{sys}}$; an extrapolation to $x_p = 0$ using the shape of the fragmentation function in JETSET 7.4 yields a total production rate of $1.200 \pm 0.037_{\text{stat}} \pm 0.082_{\text{sys}} \pm 0.070_{\text{extrap}}$ per event. The predictions of both JETSET 7.4 (1.00 η per event) and HERWIG 5.9 (1.04 η per event) are somewhat below this result. The use of the matrix elements proposed by [4] and [20] resulted in a significant effect on the momentum spectrum for low η momenta. The matrix element is not present in JETSET 7.4 and HERWIG 5.9. Published results of L3 [5] and OPAL [4] are somewhat lower than the result of this analysis.

The average ω rate per event for $x_p > 0.05$ is measured to be $0.585\pm0.019_{\text{stat}}\pm0.033_{\text{sys}}$; an extrapolation to $x_p = 0$ yields a total production rate of $0.996 \pm 0.032_{\text{stat}} \pm 0.057_{\text{sys}} \pm 0.024_{\text{extrap}}$ per event. The rate lies significantly below the prediction of JETSET 7.4 (1.31 ω per event) and somewhat below that of HERWIG 5.9 (1.13 ω per event). Published results from L3 and OPAL for the production rate of the ω are in good agreement with the result of this analysis. This measurement also agrees with that previously published in [2] and improves it substantially.

In the muonic decay mode of the ω vector meson, 18.1 ± 5.9 events are observed yielding the first measurement of the muonic branching ratio of $\text{BR}(\omega \to \mu^+\mu^-) = (9.0 \pm 2.9_{\text{stat}} \pm 1.1_{\text{sys}}) \times 10^{-5}$. The result is in agreement with the expectation from the flavour composition of the vector mesons and from lepton universality.

Acknowledgements

References

[1] For a review see A. Böhrer, Phys. Rept. **291** (1997) 107, or
I.G. Knowles and G.D. Lafferty, J. Phys. **G23** (1997) 731.

[2] ALEPH Collaboration, *Inclusive Production of Neutral Vector Mesons in Hadronic Z Decays*, Z. Phys. **C69** (1996) 379.

[3] ALEPH Collaboration, *Inclusive Production of π^0, η, $\eta'(958)$, K_S^0, and Λ in Two- and Three-Jet Events from Hadronic Z Decays*, Eur. Phys. J. **C16** (2000) 613.

[4] OPAL Collaboration, *Photon and Light Meson Production in Hadronic Z^0 Decays*, Eur. Phys. J. **C5** (1998) 411.

[5] L3 Collaboration, *Measurement of η Production in Two and Three-Jet Events from Hadronic Z Decays at LEP*, Phys. Lett. **B371** (1996) 126.

[6] L3 Collaboration, *Measurement of Inclusive ω and η' Production in Hadronic Z Decays*, Phys. Lett. **B393** (1997) 465.

[7] R. Van Royen and V.F. Weisskopf, Nuovo Cim. **A50** (1967) 617; **A51** (1967) 583.

[8] Particle Data Group, *Review of Particle Physics*, Eur. Phys. J. **C15** (2000) 1.

[9] ALEPH Collaboration, *ALEPH: A Detector for Electron-Positron Annihilations at LEP*, Nucl. Instrum. Meth. **A294** (1990) 121; **A303** (1991) 393.

[10] ALEPH Collaboration, *Performance of the ALEPH Detector at LEP*, Nucl. Instrum. Meth. **A360** (1995) 481.

[11] ALEPH Collaboration, *Measurement of the Z Resonance Parameters at LEP*, Eur. Phys. J. **C14** (2000) 1.

[12] ALEPH Collaboration, *A Precise Measurement of $\Gamma_{Z\to b\bar{b}}/\Gamma_{Z\to hadrons}$*, Phys. Lett. **B313** (1993) 535.

[13] ALEPH Collaboration, *Measurement of the B_s^0 Lifetime*, Phys. Lett. **B322** (1994) 275.

[14] T. Sjöstrand, Comput. Phys. Commun. **82** (1994) 74.

[15] J.E. Campagne and R. Zitoun, Z. Phys. **C43** (1989) 469.

[16] ALEPH Collaboration, *Studies of Quantum Chromodynamics with the ALEPH Detector*, Phys. Rept. **294** (1998) 1.

[17] G. Marchesini and B.R. Webber, Nucl. Phys. **B310** (1988) 461;
G. Marchesini et al., Comput. Phys. Commun. **67** (1992) 465.

[18] ALEPH Collaboration, *Heavy Quark Tagging with Leptons in the ALEPH Detector*, Nucl. Instrum. Meth. A346 (1994) 461.

[19] O. Krasel, *Charm-Produktion in $\gamma\gamma$-Wechselwirkungen im ALEPH-Experiment*, Diploma Thesis, Siegen University (1999).

[20] D.W. Carpenter et al., Phys. Rev. **D1** (1970) 1303.

[21] M.L. Stevenson et al., Phys. Rev. **125** (1962) 687;
J.G. Layter et al., Phys. Rev. **D7** (1973) 2565.